Synthesis of Transition-Metal-Doped $KTiOPO_4$ and Lanthanide-Doped $RbTiOAsO_4$ Isomorphs That Absorb Visible Light

Mark T. Anderson,* Mark L. F. Phillips, and Michael B. Sinclair

Sandia National Laboratories, P.O. Box 5800, Albuquerque, New Mexico 87185

Galen D. Stucky

University of California at Santa Barbara, Department of Chemistry and Materials Department, Santa Barbara, California 93106

Received July 28, 1995. Revised Manuscript Received October 10, 1995[⊗]

We have substituted aliovalent transition-metal (M = Cr, Fe, Ni, Cu, Co) and lanthanide (Ln = Er) ions that absorb visible light onto the titanium sites of the nonlinear optical materials $KTiOPO_4$ (KTP) and $RbTiOAsO_4$ (RTA). The substitution formally creates a charge deficiency on the Ti site. To compensate for this, we have substituted aliovalent counterions on the titanium (Nb), phosphorus (S, Se, Cr, Mo, W, Re), oxygen (F), or potassium (Ca, Sr, Ba, Pb) sites. The resulting new materials expand the $KTiOPO_4$ structure field for partial replacement of one or more ions. The M and Ln ions alter the optical absorption and second harmonic properties of the materials. The ions reduce the second harmonic intensities of the isomorphs (measured at 532 nm) but improve their phase-matching capabilities, allowing fundamental and second harmonic radiation to be phase matched at slightly shorter wavelengths than in the undoped host.

Introduction

Potassium titanyl phosphate ($KTiOPO_4$ or KTP) can double the frequency (halve the wavelength) of incident light essentially by coupling two photons to produce one of twice the frequency. An example is the conversion of near-IR laser light (1064 nm fundamental) to green light (532 nm second harmonic). KTP exhibits excellent chemical, physical, and optical properties (e.g., stability in ambient moisture, high damage threshold, up to 70% conversion efficiency) which have made it the frequency-doubling material of choice for many applications where coherent green light is required.[1−5]

KTP is also attractive for frequency doubling of small diode lasers to produce blue light for compact laser sources.[6] Unfortunately, at fundamental wavelengths shorter than 990 nm[7] the highly desirable situation of type II noncritical phase matching (NCPM), which allows the efficient conversion of fundamental to second harmonic light, is lost in bulk KTP crystals. The lower wavelength limit for efficient type II frequency doubling is therefore 495 nm, which is longer than is desired for compact blue laser sources.

The loss of efficient matching in bulk KTP crystals at wavelengths shorter than 990 nm is a consequence of its relatively small birefringence (Figure 1a). If the birefringence can be increased, the NCPM wavelength can be decreased (blue-shifted). Birefringence has been increased by doping KTP or its isomorphs with ions on the K or Ti sites and has been used to shorten the NCPM wavelengths of $KTiOAsO_4$:Fe[8] (−37 to 1038 nm), KTP:Na[9] (−13 to 981 nm) and KTP:Nb[10] (−102 to 892 nm) relative to the undoped host. In this work, we show that anomalous-dispersion[11] phase-matched[12] second harmonic generation (ADPM SHG)[13−15] also can be used to shorten the NCPM wavelength of KTP.

In ADPM SHG, visible light is absorbed by an ion that has been substituted into the KTP lattice. The absorption modifies the dispersion curves of KTP (Figure 1b) and shortens the wavelength at which fundamental and second harmonic light can be efficiently phase-matched.

* To whom correspondence should be addressed.

[⊗] Abstract published in *Advance ACS Abstracts,* December 1, 1995.

(1) Zumsteg, F. C.; Bierlein, J. C.; Gier, T. E. *J. Appl. Phys.* **1976**, *47*, 4980−4985.

(2) Belt, R. F.; Gashurov, G.; Liu, Y. S. *Laser Focus/Electro-Optics* **1985**, 110−124.

(3) Eimerl, D. *Proc. SPIE-Int. Soc. Opt. Eng.* **1986**, *681*, 5.

(4) Fan, T. Y.; Huang, C. E.; Hu, B. Q.; Eckhardt, R. C.; Fan, Y. X.; Byer, R. L.; Feigenlson, R. S. *Appl. Opt.* **1987**, *26*, 2391.

(5) Bierlein, J. D.; Vanherzeele, H. *J. Opt. Soc. Am. B* **1989**, *6*, 622−633.

(6) (a) Nam, D. W.; Waarts, R. G. *Laser Focus World* **1994**, *August*, 49−55. (b) Gurevich, S. A.; Portnoi, E. L.; Pronina, N. V.; Skopina, V. I. *Sov. Tech. Phys. Lett.* **1982**, *8*, 83. (c) Laurell, F.; Brown, J. B.; Bierlein, J. D. *Appl. Phys. Lett.* **1993**, *62*, 1872.

(7) For NCPM the optimum conversion efficiency is obtained with type II phase matching in the $x-y$ plane between ∼990 and 1080 nm.

(8) Loiacono, G. M.; Stolzenberger, R. A.; Loiacono, D. N. *Appl. Phys. Lett.* **1994**, *64*, 16−18.

(9) Cheng, L. K.; Cheng, L. T.; Bierlein, J. D.; Zumsteg, F. C.; Ballman, A. A. *Appl. Phys. Lett.* **1993**, *62*, 346.

(10) Cheng, L. T.; Cheng, L. K.; Harlow, R. L.; Bierlein, J. D. *Appl. Phys. Lett.* **1994**, *64*, 155−157.

(11) Normal dispersion is the increase of refractive index of the crystal as the wavelength of the incident radiation is decreased. Anomalous dispersion is the rapid decrease of refractive index as the wavelength of incident radiation increases. Anomalous dispersion occurs at and around an absorption frequency. Figure 1 illustrates normal and anomalous dispersion in KTP.

(12) A requirement for efficient production of second harmonic radiation is that the fundamental and second harmonic waves travel in phase synchronization (i.e., they are phase matched) through the transmitting medium. To meet this condition, the group velocities and thus the refractive indexes experienced by the interacting fundamental and second-harmonic waves must be identical: $n(\omega) = n(2\omega)$.

(13) Armstrong, J. A.; Bloembergen, N.; Ducuing, J.; Pershan, P. S. *Phys. Rev.* **1962**, *127*, 1918.

(14) Franken, F. A.; Ward, J. F. *Rev. Mod. Phys.* **1963**, *35*, 23.

(15) Cahill, P. A.; Singer, K. D.; King, L. A. *Opt. Lett.* **1989**, *14*, 1137−1139.

0897-4756/96/2808-0248$12.00/0 © 1996 American Chemical Society

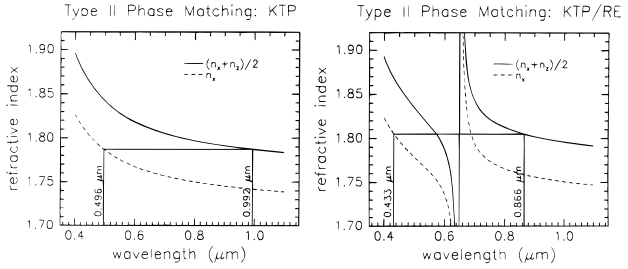

Figure 1. Normal dispersion curves for KTP (left) calculated from the Sellmeier equations.[42] The solid line is the fundamental; the dashed line is the second harmonic. Type II phase matching at 992 nm is shown. (b) Dispersion curves for KTP:Ln calculated with a Lorentzian absorption centered at 625 nm that has a linear absorption coefficient of 2×10^4 cm^{-1} and a width at half-maximum of 10 nm (right). Shown are anomalous dispersion of the fundamental and second harmonic radiation and the 126 nm blue-shift of the type II phase matching wavelength.

The larger the integrated absorption coefficient of the doped material, the larger the blue-shift of the NCPM wavelength. Thus, to maximize the blue shift, dopant ions should have large molar absorption coefficients and the host should be able to accommodate a high concentration of these ions. In addition, to achieve optimum conversion efficiency, the ions should not absorb fundamental and/or second-harmonic radiation.[16]

In an attempt to maximize blue-shift and conversion efficiency, we examined the absorption spectra and second harmonic intensities of KTP doped with transition-metal (TM) ions and $RbTiOAsO_4$ (RTA) doped with lanthanide (Ln) ions. We chose KTP as the host for transition-metal ions because $KMOXO_4$ isomorphs have a large phase field and can accommodate significant concentrations of TM ions. We chose RTA as the host for Ln ions as it offers great solid solubility of Ln than KTP. We describe two synthetic methods to produce doubly substituted KTP and RTA powders, detail the phase fields and optical properties of these materials, and demonstrate ADPM SHG.[17,18]

Experimental Section

Hydrothermal Synthesis. $KTiOPO_4$ isomorphs (KTP:M,X) were prepared from KH_2PO_4 (30 mmol), aqueous $TiCl_4$ ($5(1-x)$ mmol), $FeCl_3 \cdot 6H_2O$, $CrCl_3 \cdot 6H_2O$, $Co(NO_3)_2 \cdot 6H_2O$, $Ni(OAc)_2 \cdot 4H_2O$, or $CuCl_2 \cdot 2H_2O$ ($5x$ mmol of metal ions), KOH sufficient to neutralize the mixture (usually $20(1-x)$ mmol), 5−10 g H_2O, and stoichiometric amounts (with respect to the transition-metal ion) of WO_3, $(NH_4)_6Mo_7O_{24} \cdot 4H_2O$, or a 2-fold molar excess of KF, NH_4ReO_4, K_2SO_4, $(NH_4)_2SeO_4$, or $K_2Cr_2O_7$. $RbTiOAsO_4$ isomorphs were prepared from RbH_2AsO_4[19] (30 mmol), aqueous $TiCl_4$ ($5(1-x)$ mmol), Ln_2O_3 ($5x/2$ mmol), RbOH sufficient to neutralize the mixture (usually $20(1-x)$ mmol), 5−10 g of H_2O, and stoichiometric amounts of Nb_2O_5, $HNbCl_6$, Sb_2O_5, $RbReO_4$, WO_3, MoO_3, or a 5-fold molar excess of RbF, H_2SO_4, or 40 wt % aqueous H_2SeO_4 solution. The results section and Table 1 and 2 give specific compositions. Samples were loaded into Teflon bags (American Durafilm),

Table 1. Hydrothermal KTP:M,X: Synthetic Conditions, Maximum Cell Volumes, and LMCT Band Edge Shifts[a]

material	solid−sol (mol %)	vol[b] (Å^3)	LMCT[c] shift (nm)
KTP:Fe,			
F	100	873.9(2)	22
S	20+	870.4(8)	18
Cr	50+	882.9(3)	15
Re	15	873.9(11)	15
KTP:Cr,			
F	20+	871.3(8)	16
S	10	871.7(9)	16
Cr	2	869.8(14)	20
Se	10	874.6(8)	12
Re	<10	874.1(22)	4
Mo	<10	867.4(9)	−
W	2	870.5(26)	−
KTP:Co,			
S	20	879.6(7)	30
Re	3	872.8(13)	32
KTP:F,B	5	868.1(10)	−

[a] Note: − = not measured. Additional compositions were prepared at $x = 0.5$ and 1.00. Second harmonic relative intensities are ($x = 0.5$ and 1.0, respectively) Fe,X: X = F (0, 0); S (0, 0); Cr (2, −); Re (2, −), and F,B (8, 4). Additional KTP:Fe,X samples were prepared for $x = 0.20$. Solid solubilities and cell volumes and LMCT midpoint shifts are X = Se, 20+, 876.1 (6) (+13 nm); Mo, 10 est, 866.7 (2) (+28 nm); and W, 20+, 877.8 (3) (+19 nm). Samples KTP:M,X were prepared where $x = 0.02$, 0.05, 0.10, and 0.20. Solid solubility and maximum cell volume are Ni,X: X = F, 5, 875.5(8); S, 10, 874.4(4); Re, 5, 879.9(41) (LMCT midpoint shift + 3 nm) and KTP:Cu,X: X = F, <5, 868.7(4); S, <5, 867.7(5); Re, 2, 873.5(12) (LMCT midpoint shift + 6 nm); and Cr, 5, 872.7(4). [b] Indicates unit-cell volume at solid solubility limit. Average KTP lattice parameters are $a = 12.827(2)$, $b = 6.411(1)$, $c = 10.593(1)$ Å, and $V = 871.1(2)$ Å^3. [c] Ligand-to-metal charge-transfer band midpoint shift. LMCT midpoint for KTP is 358 nm.

Table 2. RTA:Ln,X: Synthetic Conditions and Maximum Cell Volumes[a]

material	prep	temp (°C)	time	solid−sol (mol %)	vol[b] (Å^3)
RTA:Yb,					
F	H	200	96/1	2	954.5(7)
S	H	200	96/168	<5	954.4(3)
Se	H	200	72/48	2	955.3(4)
Re	SS	850	19	2	953.6(2)
Mo	SS	800	26	2	954.3(4)
W	SS	800	24	2	955.0(2)
Nb[d]	SS	950	24	10	979.5(5)[c]
Nb	H	200	80/86	5	957.5(19)
RTA:Er,					
F	H	200	120/3	2	954.5(7)
S	H	210	120/3	2	953.6(9)
Se	H	210	120/3	2	955.3(4)
Re	H	200	96/24	2	957.4(8)
Mo	H	200	96/24	2	952.9(2)
W	H	200	96/24	<5	956.1(17)
Nb	H	200	80/86	2	954.1(2)
Nb[d]	SS	950	24	5	961.4(2)[c]
Nb[d]	SS	850	48	5+	971.4(7)[c]

[a] RTA:Ln,X (X_{Rb} = Ca, Sr, Pb, Ba) were prepared via solid-state techniques at 800 °C for 18 h. Solid solubilities are <2% in all cases. Maximum cell volumes ($x = 0.02$) are 951.3(8), 954.0(2), 955.2(2), and 953.6(2), respectively. Relative second harmonic intensities are 41, 78, 85, and 92% of RTA, respectively. [b] Indicates unit cell volume at solid solubility limit. Average RTA lattice parameters are $a = 13.258(2)$, $b = 6.680(1)$, $c = 10.767(1)$ Å, and $V = 953.5(3)$ Å^3. [c] Maximum cell volume for multiple phase samples ($x = 0.20$) are 993.8 (5) Å^3 (Yb,Nb), 978.8 (15) (Er,Nb; 950) and 979.7 (6) (Er,Nb; 850) Å^3. [d] See ref 17.

(16) KTP is transparent from 4500 to 350 nm. Absorption from ligand-to-metal charge transfer will not interfere with second harmonic generation from pump wavelengths as short as 700 nm.

(17) Anderson, M. T.; Phillips, M. L. F.; Stucky, G. D. *J. Non-Cryst. Solids* **1994**, *178*, 120−128.

(18) Phillips, M. L. F.; Anderson, M. T.; Sinclair, M. B. *Proc. Lasers 93*; Corcoran, V. J., Goldman, T. A., Eds.; STS Press: McLean, VA, 1994; pp 733−740.

(19) RbH_2AsO_4 was prepared by oxidation of As_2O_3 with 30% H_2O_2 followed by titration with RbOH. As_2O_3 (100 g) was mixed with 100 mL of H_2O in a 4 L beaker and stirred vigorously. To this a total of about 100 mL of H_2O_2 was added over 15 min as the mixture was heated (50 °C). The solution was boiled and additional H_2O_2 (50 mL) was added until all of the solid dissolved (15−30 min). The H_3AsO_4 solution was titrated to pH 6 with a 50 w/w solution of RbOH and was heated and stirred until incipient crystallization. The mixture was drowned with methanol (300 mL) and acetone (300 mL). The product was recovered by suction filtration and washed with additional methanol.

which were closed with a thermal impulse sealer (Vertrod). The samples were allowed to age at room temperature for 1−168 h. The hydrogels were autoclaved at 200 °C under autogenous pressure (200 psi) for 96−120 h. KTP isomorphs were suction filtered on paper (Whatman, medium coarse), and RTA isomorphs were suction filtered with 1.2, 0.8, 0.45, and 0.22 μm membrane filters (Micron Separations Inc.). All samples were washed with water and dried at room temperature.

Solid-State Synthesis. $RbTiOAsO_4$ isomorphs (RTA:Ln,X) were prepared from stoichiometric mixtures of RbH_2AsO_4,[19] TiO_2, Ln_2O_3 (Ln = Er, Yb), and one of the following: Nb_2O_5, Sb_2O_5, $RbReO_4$, WO_3, MoO_3, MCO_3 (M = Ca, Sr, Ba), or PbO. The results section and Table 2 give specific compositions. Samples were fired at 600 °C in platinum crucibles. After 12−24 h the samples were ground and then refired at 800−950 °C for 24−48 h.

X-ray Diffraction. Scintag PAD V and Siemens D5000 powder diffractometers were employed to collect diffraction data from 10° to 60° 2θ on polycrystalline samples. A silicon internal standard was used for each sample. Lattice parameters were determined by the use of three analysis packages: a peak fit routine, a program to correct for peak position displacement, and a least-squares lattice-parameter refinement routine. The approximate solid solubility of aliovalent ions on the titanium site was determined from plots of cell volume versus dopant concentration. The stated solid solubilities should be considered maximum, especially for values less than 5 mol %.

UV−Visible−IR Measurements. A Cary UV−visible spectrophotometer equipped with both a halogen and a tungsten lamp was used to collect diffuse reflectance spectra from 830 to 230 nm on RTA:Ln,X. A magnesium carbonate standard was used to collect a background spectrum and was mixed in a 5:1 ratio with each sample. A Cary 5E dual beam spectrophotometer equipped with a Labsphere RSA-CA-50 hemispherical reflector and a quartz halogen lamp was used to collect reflectance data from 250 to 2000 nm on KTP:M,X.

Particle Size Distribution Analysis. A Horiba Capa-700 instrument was employed to determine particle size distributions for KTP:M,X and RTA:Ln,X. Stock solutions were prepared from 10 to 15 mg of sample and 10 mL of water for RTA:Ln,X and an 85/15 w/w glycerol/water mixture for KTP:M,X. The samples were sonicated for 1 min, stirred for 10−15 min, and diluted such that their absorbance was between 0.65 and 0.95. The instrument determined absorbance versus time for a preset spin speed (9000 rpm) and time (9 min) at room temperature. Particle size distribution (volume percent) was determined from a plot of the rate of decrease of absorbance versus time, the density and viscosity of the liquid medium, and the density of the sample.

Second-Harmonic Generation. Second-harmonic intensity data were collected at 532 nm by the use of an apparatus similar to that described by Dougherty and Kurtz.[20] Aggregates of crystallites were crushed in an alumina mortar. The resulting powder was loaded into glass capillary tubes. A Quanta Ray DCR11-3D Q-switched Nd:YAG laser was used as the source of fundamental radiation. The laser produced 10 ns, 30 mJ pulses at a repetition rate of 2 Hz. Twenty pulses were averaged to quantify SH response. Relative SH responses were determined by dividing the raw second harmonic intensity of each KTP:M,X or RTA:Ln,X isomorph by the raw second harmonic intensity measured for KTP and RTA samples, respectively. The KTP and RTA standards were prepared under synthetic conditions identical to those used for the isomorphs. The second harmonic response for the most intense RTA sample was approximately 5000 times quartz for solid-state samples and 3000 times quartz for hydrothermal samples. The second harmonic response for the most intense KTP sample was approximately 6000 times quartz.

(20) Dougherty, J. P.; Kurtz, S. K. *J. Appl. Crystallogr.* **1976**, *9*, 145.

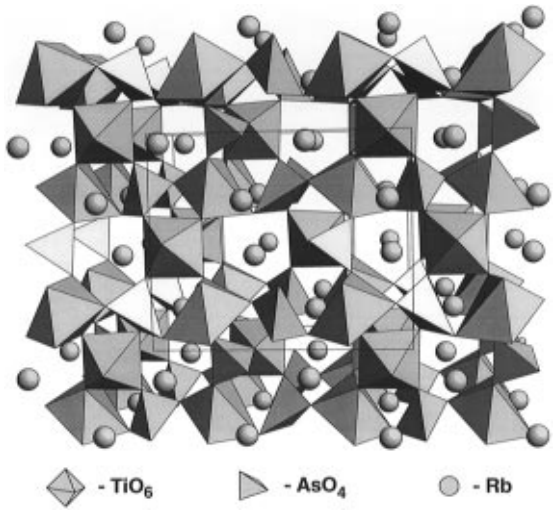

Figure 2. Structure of $RbTiOAsO_4$ viewed down [010] (space group symmetry $Pna2_1$). Dopant sites are shown in legend except for the chain oxygen sites, which occur at all linkages of two TiO_6 octahedra.

Results

Materials. $KTiOPO_4$ offers four sites for dopant ion incorporation: the K, Ti, P, and O sites (Figure 2). The general dopant schemes where M^{3+} = Fe, Cr and M^{2+} = Co, Cu, Ni, are

$$M_{Ti}',X_{Ti}^{\bullet} \quad K[Ti_{1-2x}M_x^{3+}X_x]OPO_4 \quad X_{Ti} = Nb^{5+} \tag{1}$$

$$M_{Ti}',X_P^{\bullet} \quad K[Ti_{1-x}M_x^{3+}]O(PO_4)_{1-x}(XO_4)_x \quad X_P = S^{6+}, Cr^{6+}, Se^{6+}, Mo^{6+}, W^{6+} \tag{2}$$

$$M_{Ti}',{}^1/_2X_P^{\bullet\bullet} \quad K[Ti_{1-x}M_x^{3+}]O(PO_4)_{1-x}(XO_4)_{x/2} \quad X_P = Re^{7+} \tag{3}$$

$$M_{Ti}'',2X_P^{\bullet} \quad K[Ti_{1-x}M_x^{2+}]O(PO_4)_{1-2x}(XO_4)_{2x} \quad X_P = S^{6+}, Se^{6+} \tag{4}$$

$$M_{Ti}',X_O^{\bullet} \quad K[Ti_{1-x}M_x^{3+}](O_{1-x}X_x)PO_4 \quad X_O = F^- \tag{5}$$

$$M_{Ti}'',2X_O^{\bullet} \quad K[Ti_{1-x}M_x^{2+}](O_{1-2x}X_{2x})PO_4 \quad X_O = F^- \tag{6}$$

$$M_{Ti}',X_K^{\bullet} \quad (K_{1-x}X_x)[Ti_{1-x}M_x^{3+}]OPO_4 \quad X_K = Ca^{2+}, Sr^{3+}, Pb^{2+}, Ba^{2+} \tag{7}$$

Throughout the paper, the general notation KTP:M,X (RTA:Ln,X) is used to designate the above isomorphs. The symbol M (Ln) designates a transition-metal (lanthanide) ion substituted on the Ti site; the symbol X designates ions substituted on the K, Ti, P, or O sites. In some cases a subscript is used with the X (e.g., X_P) to denote a specific site.

Schemes 1−3, 5, and 7 were used for RTA:Ln,X, where Ln is Yb^{3+} or Er^{3+}. In the case of M_{Ti}^{2+} and Re_P^{7+}, the relative ratios of aliovalent ions in Scheme 2 apply. Tables 1 and 2 show the specific compositions examined in this study.

In several cases, there is some question as to the siting of dopant ions. For example, it is conceivable based on ionic radii and coordination preferences that Ln ions could occupy the Rb or Ti site. X-ray diffraction experiments clearly showed for $(Rb_{1-2x}Ln_x)TiOAsO_4$ (x = 0.005, 0.01, 0.02, 0.05) an Ln-rich second phase occurs

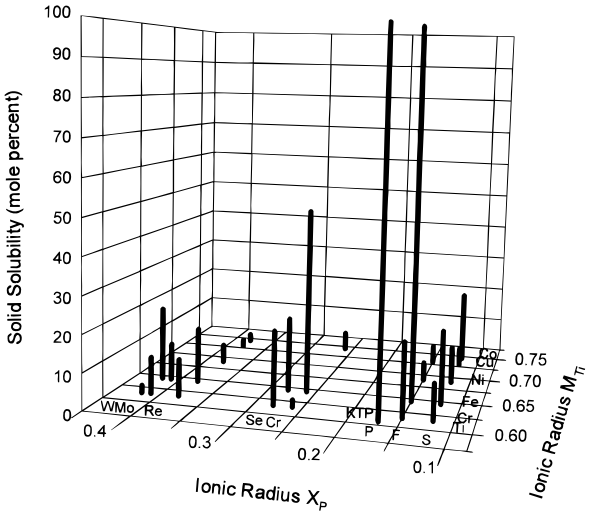

Figure 3. Solid solubility versus ionic radii M,X dopant ion pairs. For simplicity, F, which occupies an X_O site, was included on this graph. It was placed to the smaller radius side of KTP to reflect the ~5% relative ionic radius difference between F and O.

at $x = 0.01$ and there is not a statistically significant change in lattice parameter from that for $x = 0.00$ for any $x > 0.00$. The transition-metal ions W^{6+}, Mo^{6+}, and Cr^{6+} could conceivably occupy the P site or the Ti site. They were assumed to occupy the P site (as in Scheme 2) instead of forming $K_{1-2x}Ti_{1-x}M^{6+}{}_xOPO_4$ plus an anion-deficient KTP:M^{3+} phase. The latter is unlikely as the X-ray diffraction spectra did not indicate more than one KTP-like phase (for M = Cr or Fe) phase and high concentrations of anion deficiencies are unlikely in hydrothermally prepared KTP isomorphs.

Solid Solubilities. Solid solubilities for KTP:M,X are shown in Table 1 and in Figure 3. For a given X, isomorphs with M = Fe have higher solid solubilities than for any other M. In general, substitution schemes 2, 3, and 5 provide the greatest solid solubilities. Generally, ion pairs in which M and X ions are similar in size to Ti and P and differ by only one in formal charge from Ti^{4+} and P^{5+} have the highest solubilities.

Solid solubilities for RTA:Ln,X are shown in Table 2. In general, the solubilities are quite low (~2%). RTA: Ln,Nb provides the highest solid solubilities; however, it is difficult to determine accurately the solubilities for this scheme from lattice parameter changes. In this system, the lattice parameters continue to increase even after the solubility limit of Ln (x_{max}) has been reached. Nb continues to be incorporated into the host as the phase $Rb_{1-y}[Ti_{1-2xmax-y}Ln_{xmax}Nb_{xmax+y}]OAsO_4$ forms. The ionic radius of Nb is greater than Ti so the lattice parameters continue to increase. The solid solubilities of Ln in RTA:Ln,Nb are estimated solely from the appearance of Ln-rich second phases in the X-ray diffraction spectra, and the stated limits may overestimate the actual solubilities.

UV−Visible Spectra. RTA:Ln,X exhibit absorption spectra with sharp, narrow bands characteristic of the lanthanide ion incorporated into the host (Figure 4a). In general these bands do not overlap fundamental or second-harmonic frequencies. For undoped RTA the midpoint of the ligand-to-metal charge-transfer (LMCT) band occurs at 330 nm and there are no absorption bands in the visible region of the spectrum. RTA:Er,X

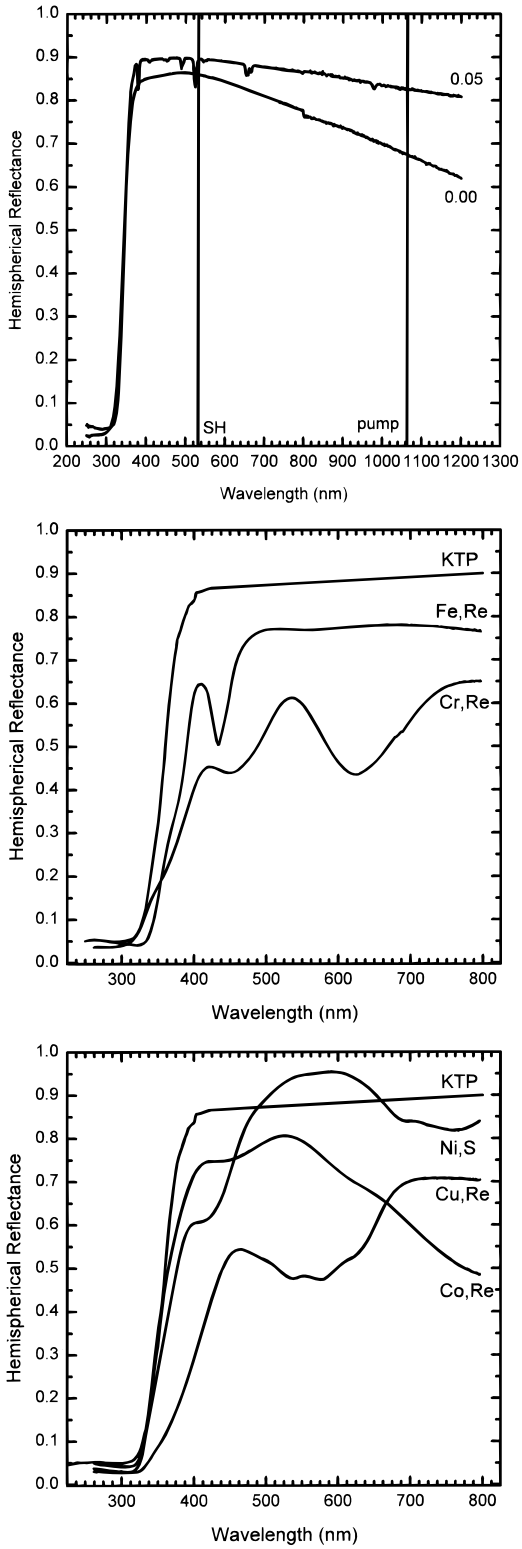

Figure 4. Representative UV−visible spectra of (a, top) $Rb[Ti_{1-x}Er_x]O(AsO_4)_{1-x}(WO_4)_x$ for $x = 0.00$ and 0.05, (b, middle) KTP:M,X where dopant concentrations are 5% for Cr and 10% for Fe, and (c, bottom) KTP:M,X where dopant concentrations are 5% for Co and Cu and 10% for Ni.

samples show −3 to 20 nm red shifts of the LMCT band midpoint and exhibit absorption maxima in the visible spectrum at 379, 408, 423, 488, 493, 524, 544, 653, 657, and 665 nm. Generally, materials prepared hydrothermally display smaller shifts of the LMCT band than those prepared via high-temperature techniques.

KTP:M,X exhibit broad absorption bands in the visible region of the spectrum (Figure 4b,c). These bands do

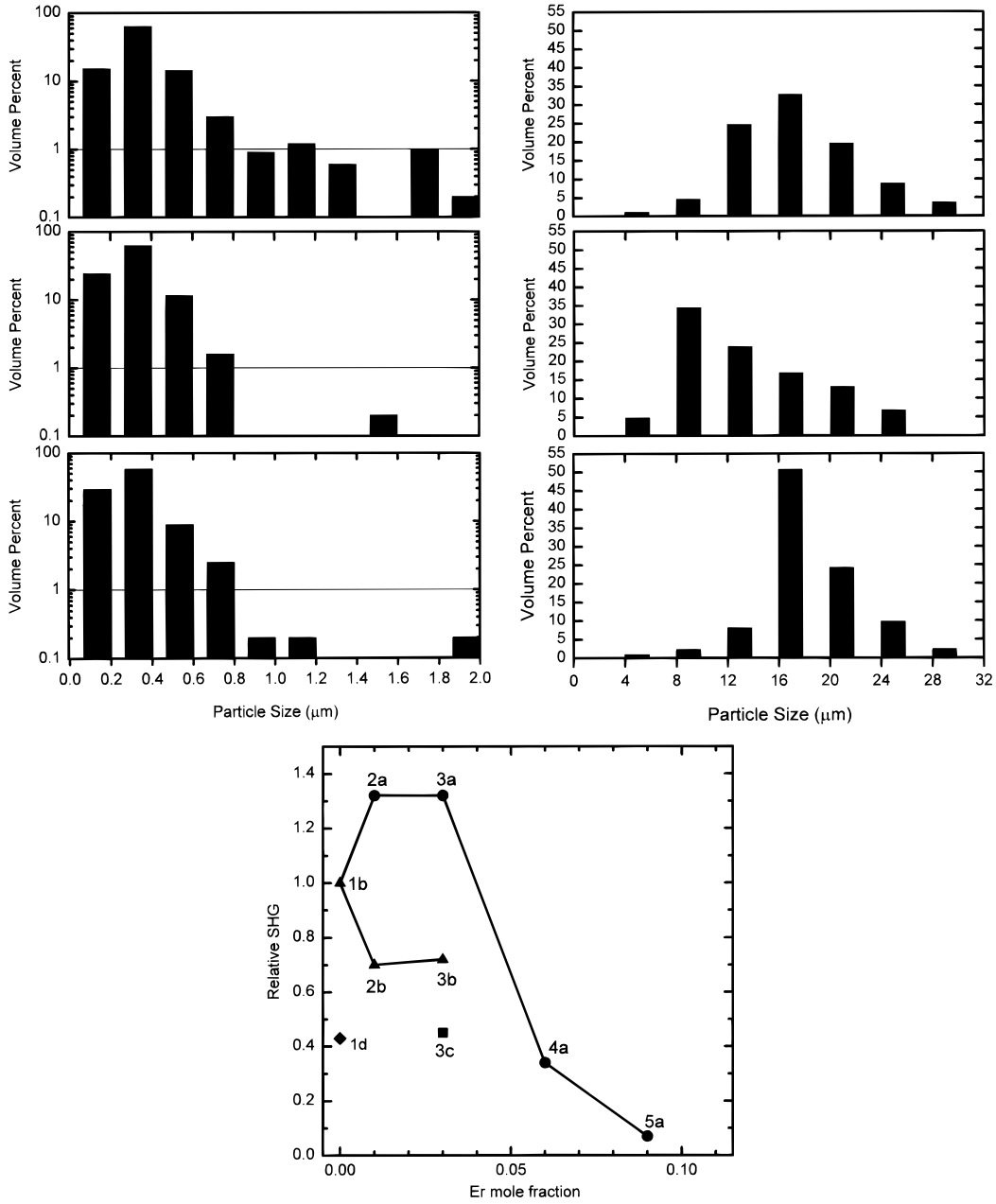

Figure 5. (a, top left) Particle size distributions (psd) for $Rb[Ti_{1-x}Er_x]O(AsO_4)_{1-x}(SO_4)_x$. Initially five samples (x = 0.00, 0.01, 0.03, 0.06, 0.09; numbered 1−5 were filtered sequentially through 1.2 (a), 0.8 (b), 0.45 (c), and 0.22 μm (d) membranes. This generated four fractions (a−d) for each sample (20 fractions in all). The psd of three of the fractions (1b, bottom, r_{ave} = 0.25 (18); 2a, middle, r_{ave} = 0.26 (13); and 2b, top, r_{ave} = 0.29 (24)) are shown. Each bar represents the volume fraction of particles in the 0.2 μm interval it is between. (b, top right) Relative second harmonic generation intensities for several of the samples (note: for sample 3a, r_{ave} = 0.38 (25); for sample 4a, r_{ave} = 0.72 (34)). Not all fractions contained enough sample to perform psd and SH intensity measurements. (c, bottom) Particle size distribution for KTP (bottom), KTP:Cr,S (middle), and KTP:Co,S (top). Each bar represents the volume fraction of particles in the 4 μm interval it is between.

overlap the fundamental and/or second-harmonic frequencies. The midpoint of the LMCT band is 358 nm for undoped KTP.

The midpoint of the LMCT band in KTP:Fe,X is red-shifted 13−28 nm relative to KTP (Table 1), with a second band at 430−436 nm, depending on the identity of X. This second band is so close to the LMCT band that second-harmonic light generated at a frequency between the two bands would be significantly attenuated and may cause significant heating of the material.

The midpoint of the LMCT band in KTP:Cr,X is red-shifted 4−20 nm, depending on the identity of X. There are also two strong absorption bands in the visible with maxima at 446−452 and 620−628 nm. Again the band is not favorably placed to allow efficient transmission of blue second-harmonic frequencies.

KTP:M,X exhibit broad absorption bands for M = Cu (550−1400 nm), Ni (600−1600 nm), and Co (410−660 nm). These bands overlap fundamental and/or second harmonic wavelengths needed to produce blue light.

Mineral Chemistry and Particle Size Distribution. The effect of a mineralizer on median particle size and particle size distribution is demonstrated by the RTA:Er,S series (Figure 5a). The particle size increases significantly as dopant concentration (x) increases (at x = 0.00, r_{median} = 0.25 (18) and for x = 0.6, r_{median} = 0.72 (34)) as does the breadth of the distribution. A similar increase in particle size is observed in hydrothermal

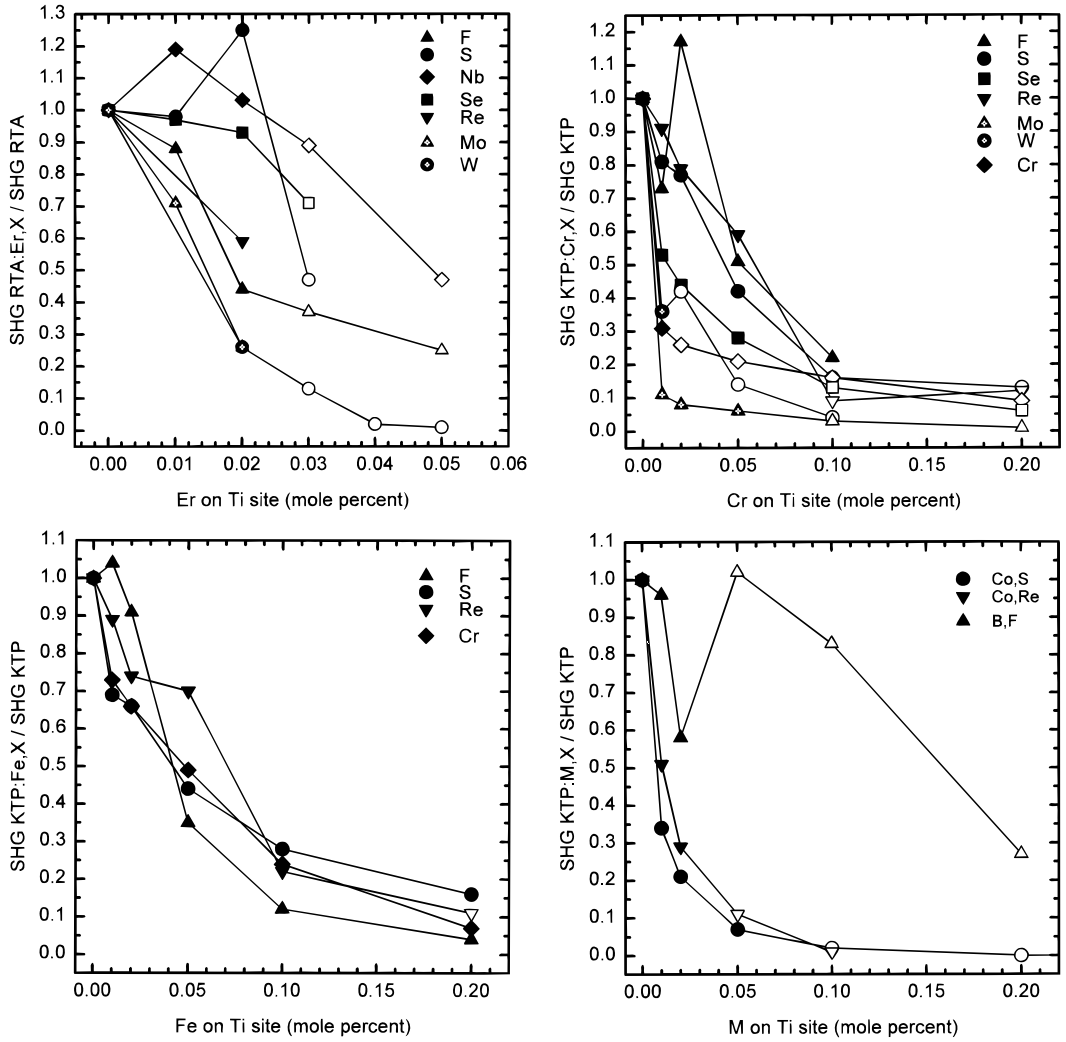

Figure 6. Relative second harmonic generation intensity at 532 nm for (a, top left) RTA:Er,X, (b, bottom left) KTP:Fe,X, (c, top right) KTP:Cr,X, (d, bottom right) KTP:M,X. Relative errors are ±20%. Open symbols represent compositions for which the solid solubility limit of dopants in the host has been exceeded.

RTA:Ln,X samples prepared in the presence of selenate, chloride, and fluoride ions.

The particle size for hydrothermally prepared KTP samples is nearly an order of magnitude larger than for RTA (Figure 5c).[21] In contrast to the RTA:Ln,S systems, the KTP:M,S samples have smaller particle sizes than the parent. Differences in mineralizer concentration (2 versus 5 times absorber ion concentration) and source, room-temperature aging time, and particulate versus molecular source of dopant ions may account for the relative change in particle size from the parent for doped RTA versus doped KTP.

Second Harmonic Generation. Figure 6 shows that the second harmonic intensity generally decreases with dopant ion concentration for RTA:Er,X and KTP:M,X. At low dopant concentrations, RTA:Er,X samples prepared in the presence of the mineralizers sulfate, selenate, chloride, and fluoride ion do not follow this general trend (discussed below).

(21) The marked difference in average particle size of hydrothermally prepared KTP and RTA implies that either the nucleation or growth of RTA is much slower than for KTP. In addition, the alkali-metal ion seems to contribute to particle size. Attempts to prepare crystalline $CsTiOAsO_4$ samples yielded only extremely small amorphous particles.

Discussion

KTP Structure Field. Figure 7a shows the structure field for $KTiOPO_4$ isomorphs in which at least one ion has been completely replaced (e.g., K**Sn**OPO_4 or **NaGe**OPO_4). The general formula of the compounds is M′MOXO_4, where M′, M, and X designate the K-, Ti-, and P-site ions, respectively. Several M′MXPO_4 and M′M$XAsO_4$ isomorphs are also included. A projection of the structure field onto the M,X_p axes is shown in Figure 7b. The projection shows clearly that the smaller the M′ ion, the smaller the M and X ions that can be completely substituted into the host (e.g., for M′ = Na, M = Ge but not Sn), and the larger the M′ ion, the larger the M and X ions that can be completely substituted into the host (e.g., for M′ = Rb, M = Sn but not Ge).

Owing to the much larger ionic radius of Ln versus Ti ions, a host with a larger M′ ion than K and a larger X ion than P was chosen as the host for Ln ions, i.e., $RbTiOAsO_4$. Owing to the large size of the M′ = K structure field, KTP was chosen as the host for transition-metal dopants.

Solid Solubility of Aliovalent Ions in KTP and RTA. The solid solubility of dopant ions in KTP and RTA depends critically on their size and charge. Figure 8 shows the K$MOXO_4$ field for previously known ma-

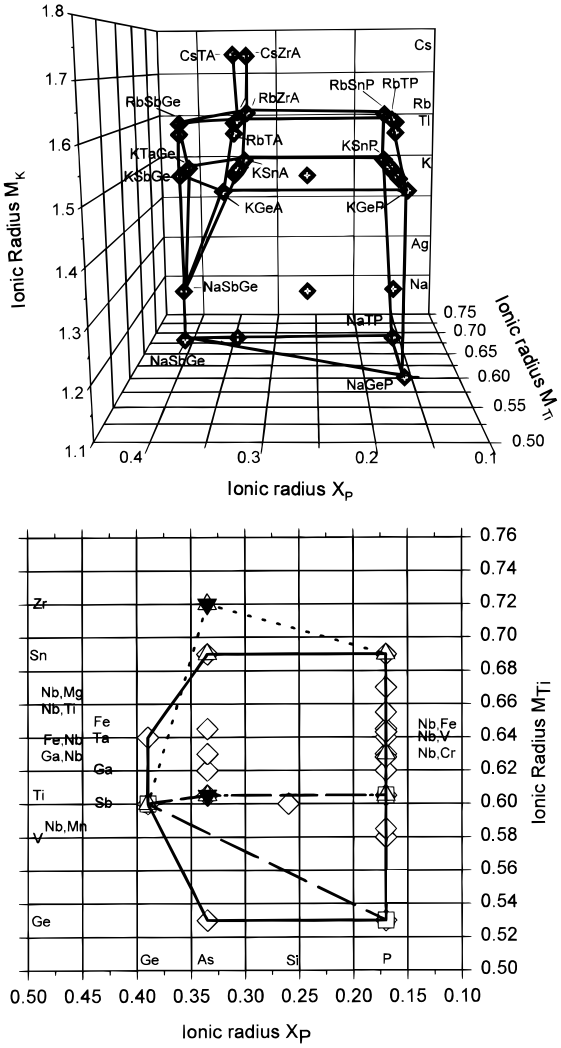

Figure 7. (a, top) Structure field for $KTiOPO_4$ isomorphs ($M'MOXO_4$). The diamonds indicate compounds for which at least one of the host ions in KTP had been completely replaced. KTP lies along the horizontal line between KSnP and KGeP. Materials that have partial replacement of one or more ions are not shown. Compounds with X_O = F are included. They are plotted according to their M′, M, and X_p ionic radii. Compounds included are Na−$NaTiOPO_4$,[43] $NaTiOAsO_4$,[44] $NaGeOPO_4$,[35] $NaSbOGeO_4$,[45] Ag−$AgTiOPO_4$,[35] $AgSbOGeO_4$,[45] $AgSbOSiO_4$,[45] K−$KGeOPO_4$[46] $KVOPO_4$,[35] $KMn_{0.5}Nb_{0.5}OPO_4$,[25a] $KGa_{0.5}Nb_{0.5}OPO_4$,[25a] $KTiOPO_4$,[40] $KGa(F_{0.7}OH_{0.3})PO_4$,[35] $KFe_{0.5}Nb_{0.5}OPO_4$,[35] $KMg_{0.33}Nb_{0.67}OPO_4$,[38] $KSnOPO_4$,[36] $KSbOSiO_4$[47] $KGeOAsO_4$,[25a] $KTiOAsO_4$,[48,49] $KGaFAsO_4$,[25a] $KGa_{0.5}Nb_{0.5}OAsO_4$,[25a] $KFeFAsO_4$,[25a] $KSnOAsO_4$,[25a] $KSbOGeO_4$,[50] $KTaOGeO_4$,[51] $KNb_{0.5}Ti_{0.5}OPO_4$,[52] $KNb_{0.5}V_{0.5}OPO_4$,[52] $KNb_{0.5}Cr_{0.5}OPO_4$,[52] $KNb_{0.5}Fe_{0.5}OPO_4$,[52] $KTa_{0.5}Ti_{0.5}OPO_4$,[52] $KTa_{0.5}V_{0.5}OPO_4$,[52] $KTA_{0.5}Cr_{0.5}OPO_4$,[52] $KTa_{0.5}Fe_{0.5}OPO_4$,[52] Tl−$TlTiOPO_4$,[53,54] $TlTiOAsO_4$,[47,48] $TlSbOGeO_4$,[49] Rb−$RbTiOPO_4$,[51,55] $RbGa_{0.5}Nb_{0.5}OPO_4$,[25a] $RbSnOPO_4$,[35] $RbTiOAsO_4$.[474,8] $RbZrOAsO_4$,[25a] $RbSbOGeO_4$,[49] Cs−$Cs_{0.5}Rb_{0.5}TiOAsO_4$,[25a] $CsTiOAsO_4$,[48,56] $CsZrOAsO_4$.[37] (b, bottom) M,X projection of $M'MOXO_4$ structure field onto the M,X axes for M′ = Na (large dash, boxes), K (solid line, diamonds), Rb (fine dash, triangles), and Cs (inverted solid triangles). This figure is simply Figure 7a viewed from the top. Identity of $M'MOXO_4$ can be determined from symbols, M and X ions listed on axes, and figure caption 7a.

terials and for isomorphs in this study. All KTP:M,X examined here, except for $KFeFPO_4$[22] and $KFeOXO_4$, where X = Cr, Se, lie outside the $KMOXO_4$ structure field for isovalent ions (Figure 8, large dashed line). Consequently all KTP:M,X isomorphs, except $KFeFPO_4$, have solid solubilities of M and X less than 100%. Ln

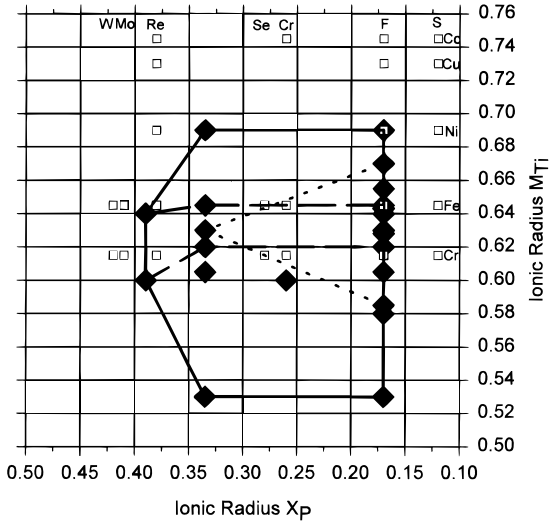

Figure 8. M,X projection of the $KMOXO_4$ structure field for substitutions on the Ti site: (1) isovalent (solid lines), (2) aliovalent M_1,M_2 pairs (small dashed lines), and (3) aliovalent M plus X (large dashed lines). Open boxes show the KTP: M,X phases reported here; M and X ions are shown on the right and top axes. Isomorphs that contain F are plotted according to their M′, M, and X_p radii.

ions (ionic radii greater than 0.86 Å)[23] lie far from the 100% solubility field for $M'MOXO_4$ and thus have low solid solubilities in RTA.[24]

Nonlinear Optical Properties of KTP and Isomorphs. There is a wealth of knowledge, both experimental and theoretical, about the nonlinear optical properties (NLO) of KTP and isomorphs.[25a,b] We will summarize this information and, in this context, draw conclusions about the NLO properties of KTP:M,X and RTA:Ln,X.

First, it is necessary to address the effect of preparation conditions on second harmonic intensity and perceived nonlinear optical behavior.

Effect of Sample Preparation Conditions on Second Harmonic Generation Intensity. The measured second harmonic generation intensity, $\mathbf{P}(2\omega)$, of powdered samples is affected by the intrinsic second-order nonlinear optical coefficients of the materials as well as crystallite size effects. Three factors influence the latter:[26] average crystallite size (r_{ave}), coherence length (l_{coh}), and number of crystallites (N) illuminated by the fundamental radiation.

Kurtz[33] showed that for particles that have $r_{ave} \ll l_{coh}$ (l_{coh} is typically a few millimeters in KTP) the second harmonic output, $\mathbf{P}(2\omega)$, increases almost linearly with r_{ave}. In the samples in the present study, many of the crystallites have $r_{median} \ll l_{coh}$ and are assumed to be phase matched. In addition, the r_{median} in mineralized samples changes with dopant concentration (x). Therefore, we expect an increase in $\mathbf{P}(2\omega)$ with x (of course,

(22) Matvienko, E. N.; Yakubovich, O. V.; Simonov, M. A.; Belov, N. V. *Dokl. Akad. Nauk SSSR* **1979**, *247*, 875−878.
(23) Shannon, R. D. *Acta. Crystallogr., Sect. A* **1976**, *32*, 751−767.
(24) In an attempt to increase Ln solubility, several experiments were conducted to examine M′ = Cs. In general, for solid-state reactions, mixed phase samples formed that included a high-temperature CTA polymorph; hydrothermal preparations yielded only very small particles that were amorphous to X-ray diffraction.
(25) (a) Stucky, G. D.; Phillips, M. L. F.; Gier, T. E. *Chem. Mater.* **1989**, *1*, 492−509. (b) Hagerman, M. E.; Poeppelmeier, K. R. *Chem. Mater.* **1995**, *7*, 602−621.
(26) Kurtz, S. K. *IEEE J. Quantum Electron.* **1968**, *QE-4*, 578.

this assumes that the second-order nonlinear optical coefficients do not change with r_{ave}).

The mineralized RTA:Ln,X do exhibit an increase in $\mathbf{P}(2\omega)$ with x, but only at very low x. At higher concentrations, the $\mathbf{P}(2\omega)$ rapidly decreases. For example, the maximum in the $\mathbf{P}(2\omega)$ versus x curve occurs at 2% for RTA:Er,S (Figure 6a) and at higher concentrations $\mathbf{P}(2\omega)$ decreases rapidly.

The most interesting and important regime for RTA:Er,S is $x < 3\%$, where the samples are single phase and $\mathbf{P}(2\omega)$ is a maximum. The key question is whether the increase in $\mathbf{P}(2\omega)$ reflects an increase in NLO coefficients or is simply an effect of increased particle size. To examine the magnitude of intrinsic nonlinear optical coefficients more directly, we attempted to eliminate particle size effects. We obtained fractions from doped (2b) and undoped samples (1b) that have very similar median particle sizes and distributions (Figure 5a). When their $\mathbf{P}(2\omega)$s are compared (Figure 5b) the doped sample is less than that of undoped RTA. The increase with x in $\mathbf{P}(2\omega)$ for doped versus undoped RTA:Er,S in Figure 6a is simply an effect of the larger median crystallite sizes in the doped material, and we conclude that the intrinsic nonlinear optical coefficients for the doped samples are less than for the parent. Furthermore we believe that this is the case for all of the mineralized samples, and that the increase in $\mathbf{P}(2\omega)$ at low concentrations for these samples is also an effect of particle size rather than increased NLO coefficients.

Optical Nonlinearity in KTP and Isomorphs. Several authors conclude that NLO properties of KTP are primarily associated with the electronic and structural properties of TiO_6 groups[27−32] as well as longer range interactions in the Ti−O═Ti−O chains.[33] It is clear from these treatments that at least three interrelated properties contribute to the nonlinear properties of KTP and isomorphs: the electronic configuration of M, the distortion of the MO_6 unit, and the extent of uninterrupted Ti−O═Ti−O chains.

Electronic Configuration of Dopant Ions and SH Intensities of KTP Isomorphs. Single-crystal studies on $KFeFPO_4$,[34] $KGaF_{0.7}(OH)_{0.3}PO_4$,[35] $KTi_{1-x}Sn_xOPO_4$,[36] $CsZrOAsO_4$,[37] and $K(Mg_{1/3}Nb_{2/3})PO_5$,[38] which contain $3d^5$, $3d^{10}$, $4d^{10}$, and $4d^0$ valence orbitals, show that the environment around the M ions is significantly less distorted[39] from octahedral than in KTP[40] and that SH responses are dramatically attenuated.[41] The lengthening of the shortest M−O bonds and sharply decreased SH responses in these isomorphs, as compared to KTP, are attributable, at least in part, to electronic effects.

The distortion of TiO_6 groups in KTP has been ascribed to a stabilization of a distorted ground state formed by mixing orbitals of metal dπ and oxygen pπ symmetry. The mixing introduces a finite amount of charge-transfer excited-state character into the valence-band orbitals, as defined by the mixing coefficients. The coefficients are influenced by the magnitudes of the bandgap and the overlap integrals. The mixing coefficients determine the degree of distortion and the molecular hyperpolarizability of the MO_6 groups.

The antibonding character of partially filled M atom orbitals[44−46] results in (1) decreased distortion of the MO_6 group, (2) reduced mixing of the metal dπ and oxygen pπ orbitals, (3) decreased molecular hyperpolarizability (β_{ijk}) of the MO_6 unit, and (4) decreased favorable long-range intrachain interactions ($\beta_{||}$) by interrupting the Ti−O═Ti−O chains. These factors contribute to a pronounced reduction in the second-order nonlinear coefficient $\chi^{(2)}_{ijk}$ and the optical nonlinearity.

In addition to the above examples, it has been shown that complete substitution of Ti by isovalent or aliovalent main-group ions or ion pairs (Ge, Sn; Ga, Nb; Ga, F)[35] or by transition-metal ions or ion pairs (V, Zr, Fe, Nb; Mn, Nb)[35] also results in a dramatic decrease of SH intensity (to less than 0.001 times that of KTP). Note that KVP absorbs light at second-harmonic frequencies (532 nm for Nd:YAG), so the effects of the d^1 electronic configuration on SH intensity have not been determined unambiguously. It is suspected that the effects are minimal because the V═O bond in KVP is slightly shorter than the Ti═O bond in KTP.

(27) Bergman, J. G.; Crane, G. R. *J. Solid State Chem.* **1975**, *12*, 172−175.
(28) Levine, B. F. *Phys. Rev. B* **1974**, *10*, 1655.
(29) Levine, B. F. *Phys. Rev. B* **1973**, *7*, 2600−2625.
(30) Chen, C.-T. *Annu. Rev. Mater. Sci.* **1986**, *16*, 203−243 and references therein.
(31) Phillips, M. L. F.; Harrison, W. T. A.; Gier, T. E.; Stucky, G. D.; Kulkarni, G. V.; Burdett, J. K. *Inorg. Chem.* **1990**, *29*, 2158.
(32) Munowitz, M.; Jarman, R. H.; Harrison, J. F. *Chem. Mater.* **1993**, *5*, 1257−1267.
(33) Munowitz, M.; Jarman, R. H.; Harrison, J. F. *Chem. Mater.* **1993**, *5*, 661−671.
(34) Belokoneva, E. L.; Yakubovich, O. V., Tsirelson, B. G. Urosov, V. C. *Neorg. Mater.* **1990**, *26*, 595−601.
(35) Phillips, M. L. F.; Gier, T. E.; Eddy, M. M.; Keder, N. L.; Stucky, G. D.; Bierlein, J. D. *Solid State Ionics* **1989**, *32/33*, 147−153.
(36) Phillips, M. L. F.; Harrison, W. T. A.; Stucky, G. D. *Inorg. Chem.* **1990**, *39*, 3245−3247.
(37) Phillips, M. L. F.; Harrison, W. T. A.; Stucky, G. D. *J. Opt. Mater.*, submitted.
(38) McCarron, E. M., III; Calabrese, J. C.; Gier, T. E.; Cheng, L. K.; Foris, C. M.; Bierlein, J. D. *J. Solid State Chem.* **1993**, *102*, 354−361.
(39) The range of Ti−O bonds in KTP for Ti(1) and Ti(2) is 1.72−2.16 and 1.74−2.10 Å, respectively. The range of M−O bond lengths in the above mentioned materials for M(1) and M(2) is in KTP:Fe,F, 1.96−2.05 and 1.92−2.03 Å; in KTP:Ga(F,OH), 1.91−1.94 and 1.93−1.98 Å; in KTP:Sn 1.97−2.11 and 1.96−2.09 Å; in CTA:Zr, 1.96−2.21 and 2.01−2.18 Å, and in KTP:Mg,Nb, 1.89−2.12 Å (space group symmetry $P4_122$).
(40) Tordjman, I.; Masse, R.; Guitel, J. C. *Z. Kristallogr.* **1974**, *139*, 103−115.
(41) For example, in KTP:Ga,(F,OH) at $x = 0.10$, the relative SH intensity is 81%, and at $x = 0.20$ is 31% of that for KTP; for KTP:Mg,-Nb at $x = 0.1$, the relative SH response is less than 5% of KTP; and for KTP:Sn at $x = 0.10$, the relative SH intensity is 57% of KTP.
(42) Vanherzeele, H.; Bierlein, J. D.; Zumsteg, F. C. *Appl. Opt.* **1988**, *27*, 3314−3316.
(43) Phillips, M. L. F.; Harrison, W. T. A.; Gier, T. E.; Stucky, G. D. *Proc. SPIE−Int. Soc. Opt. Eng.* **1989**, *225*, 1104.
(44) Phillips, M. L. F.; Harrison, W. T. A.; Stucky, G. D.; McCarron, E. M., III; Calabrese, J. C.; Gier, T. E. *Chem. Mater.* **1992**, *4*, 222−233.
(45) Mill, B. V.; Butashin, A. V.; Stefanovich, S. Yu. *Zh. Neorg. Khim.* **1993**, *38*, 947−949.
(46) Avduevskaya, K. A.; Tananaev, I. V.; Mironova, V. S. *Izv. Akad. Nauk SSSR, Neorg. Mater.* **1965**, *1*, 894−899.
(47) Crosnier, M.-P.; Guyomard, D.; Verbaere, A.; Piffard, Y. *Eur. J. Solid State Inorg. Chem.* **1990**, *27*, 845−854.
(48) El Brahimi, M.; Durand, J. *Rev. Chim. Mineral* **1986**, *23*, 146−153.
(49) El Haidouri, A.; Durand, J.; Cot, L. *Mater. Res. Bull.* **1990**, *25*, 1193−1202.
(50) Belokoneva, E. L.; et al. *Neorg. Mater.* **1991**, *27*, 1708−1712.
(51) Belokoneva, E. L.; et al. *Zh. Neorg. Khim.* **1992**, *37*, 998−1003.
(52) Gopalakrishnan, J.; Kasthuri Rangan, K.; Raghavendra Prasad, B.; Subramanian, C. K. *J. Solid State Chem.* **1994**, *111*, 41−47.
(53) Masse, R.; Grenier, J. C. *Bull. Soc. Fr. Mineral Cristallogr.* **1971**, *94*, 437.
(54) Harrison, W. T. A.; Gier, T. E.; Stucky, G. D.; Schultz, A. J. *J. Chem. Soc., Chem. Commun.* **1990**, 540−542.
(55) Thomas, P. A.; Mayo, S. C.; Watts, B. E. *Acta Crystallogr., Sect. B* **1992**, *48*, 401−407.
(56) Cheng, L. T.; Cheng, L. K.; Bierlein, J. D.; Zumsteg, F. C. *Appl. Phys. Lett.* **1993**, *63*, 2618−2620.

NLO Properties of KTP:M,X and RTA:Ln,X. We find a general decrease in SH intensity versus x regardless of the identity of the M or Ln ion in KTP:M,X and RTA:Ln,X (when particle size effects are considered). We find no general trends in SH behavior with the identity of X and conclude that its identity does not have a significant effect on intrinsic SH behavior but that its identity can affect particle size and measured SH intensities.

We attribute the general decrease in SH response in KTP:M,X and RTA:Ln,X, as in other isomorphs,[43−46] to the interrelated factors (1) the decreased overlap of metal dπ and oxygen pπ orbitals that occurs when the metal d orbitals are partially filled. (The Yb and Er ions are $4d^{10}$ and the M ions are $3d^3$, $3d^5$, $3d^7$, $3d^8$, and $3d^9$ for Cr(III), Fe(III), Co(II), Ni(II), and Cu(II). It is less energetically favorable to substantially mix the metal dπ and oxygen pπ orbitals in these partly filled configurations and to distort the coordination sphere as compared to a $3d^0$ or $3d^1$ configuration (as in KTP or $KVOPO_4$).) (2) Interruption of the extended Ti—O═Ti—O chains by dopant metal atoms on the Ti site. (3) For KTP:M,X (M = Cr, Co, Cu, Ni) increased absorption of fundamental and/or second harmonic light as the concentration of the absorber ion is increased.

NCPM Wavelength. Dopant ions that absorb visible light provide anomalous dispersion and alter the NCPM wavelength (Figure 1b). All of the dopant ions studied here were successfully incorporated into KTP or RTA and thus serve to demonstrate the concept of ADPM SHG. Beyond demonstrating the concept, in order to effect a substantial shift in NCPM wavelength via anomalous dispersion and maintain a high conversion efficiency, two criteria must be satisfied: the introduced absorption must have a high oscillator strength, and the doped material must be transparent at the fundamental and second harmonic frequencies. Despite successful incorporation of many dopant pairs, simultaneous satisfaction of both criteria has not been achieved with any doping scheme owing to low intensity of the absorption bands in doped RTA and to the broad-band absorptions in doped KTP (M = Cr, Co, Cu, Ni). As a result, calculations demonstrate that the shift of noncritical phase-matching wavelength owing to anomalous dispersion, as determined from absorbance measurements on RTA:Er,X (X = Nb(V), F, Mo(VI), W(VI)) and KTP:M,X (Co, Re; Fe, F) single crystals,[18] is less than 1 nm.

Conclusions

$KTiOPO_4$ and $RbTiOAsO_4$ can host a wide variety of aliovalent ions. The KTP structure field (less than 100% substitution) has been significantly expanded with the RTA:Ln,X compositions reported here. The solid solubilities of the dopant ions examined here are generally low because they are isovalent and have significant size mismatches with host ions. The concentration of the M and Ln dopant ions in the host strongly influences the SH intensities and the magnitude of the NCPM wavelength shift. The counterions (X) influence solid solubilities of ion pairs, but little affect absorption or second harmonic properties. The M and Ln dopant ions provide anomalous dispersion and blue-shift the type II NCPM wavelength relative to the host. The blue shift is less than 1 nm for all isomorphs. Ion pairs that do not absorb fundamental or SH radiation (Er with S, F, Se, Re, Mo, W, Nb) or that have high solid solubilities and intense absorption bands (Cr, F; Co, S) will be most beneficial to phases matching at shorter wavelengths.

Acknowledgment. This work was funded by the United States Department of Energy under Contract Number DE-ACO4-94AL-85000 and by the National Science Foundation under Contract Number DMR-9520971. We thank Vojislav Srdanov of the University of California at Santa Barbara and Herb Tardy, Lloyd Irwin, and Diana L. Lamppa of Sandia National Laboratories for their technical assistance.

CM950352I